



## Shape engineering of palladium aerogels assembled by nanosheets to achieve a high performance electrocatalyst



Mehdi Zareie Yazdan-Abad\*, Meissam Noroozifar\*, Abdollah Shafaei Douk,  
Ali Reza Modarresi-Alam, Hamideh Saravani

Department of Chemistry, University of Sistan and Baluchestan, P.O. Box 98135-674, Zahedan, Iran

### ARTICLE INFO

**Keywords:**  
Palladium aerogel  
Palladium nanosheets  
Self-assembly  
Ethanol oxidation

### ABSTRACT

Three-dimensional noble metal aerogels are unique solid materials with ultralow densities, large open pores, and high surface areas. Despite several research works on noble metal aerogels assembled by nanochains, the investigation of noble metal aerogels assembled by nanosheets has not been reported to date. In this work, palladium aerogels assembled by nanosheets have been synthesized in four various carboxylic acid (RCOOH) solvents with different alkyl groups ( $R = H$ – (formic acid, FA),  $CH_3$ – (acetic acid, AA),  $CH_3CH_2$ – (propionic acid, PA), and  $CH_3CH_2CH_2$ – (butyric acid, BA)). It has been found that the  $R$  groups play a crucial role in the morphology of palladium aerogels so that the Pd aerogels synthesized in acetic acid and propionic acid solvents show better morphology than that of palladium aerogels synthesized in formic acid and butyric acid solvents. The electrocatalytic activity and durability of all aerogels are evaluated using cyclic voltammetry (CV) and chronamperometry (CA) experiments toward ethanol oxidation. Based on CV and CA data, Pd aerogels synthesized in AA and PA show high catalytic activity and durability due to their unique structures.

### 1. Introduction

Synthesis of unsupported nanocatalysts with high surface area and large porosity has aroused significant interest in nanotechnology. Recently, unsupported electrocatalysts have been promoted by Company 3 M for polymer electrolyte fuel cells [1]. In commercial catalysts such as Pd/C, the corrosion of the carbonaceous support during the operation of fuel cell leads to loss of noble metal nanoparticles; hence, as time goes by, the activity of the catalyst is dramatically reduced [2]. Therefore, a wealth of studies focused on solving this problem. It has proved that self-assembly processes are the most powerful strategies for the creation of self-supported three dimensional (3-D) materials with unique structures (e.g. large surface area, abundance active sites, and high porosity) which can be applied as supportless electrocatalysts [3–6]. Among the 3-D nanostructures, noble metal aerogels (NMAs) are very promising un-supported electrocatalysts that have ultra-low densities, high inner surface areas and large open pores [7–16]. In recent years, a variety of methods have been reported for the fabrication of NMAs, while the development of self-assembled NMAs has significantly slowed down because of the same structures. Since in all previous studies NMAs have been assembled only by nanochains, to develop this field, it is an urgent to

introduce a new structure of NMAs. After the introduction and several studies on the NMAs assembled by nanochains, now it is time to introduce and study the new generation of NMAs. Compared to the nanochains, two-dimensional (2-D) nanosheets with atomic thickness, not only provide high surface area and high flexibility but also possess outstanding electrical conductivity and atom utilization efficiency [17]. Therefore, nanosheets are promising candidates to create the new generation of NMAs, unfortunately, they are prone to stacking due to the strong interlayer interactions, which can greatly decrease the surface area. Therefore, rational engineering of 2-D nanosheets into 3-D aerogels is necessary to prevent the stacking. Moreover, it is known that the size of the nanosheets affect the density and pore size distribution of the aerogels so that the smaller size of nanosheets leads to the smaller pore size and higher density in the aerogels [18]. In this regard, our research team made extensive studies on the synthesis of Pd aerogels assembled by extensive and ultrathin nanosheets using a surfactant free route.

In the present study, a new class of the Pd aerogels with different morphology was synthesized using monocarboxylic acid (RCOOH) solvents, with different alkyl groups ( $R = H$ – (formic acid, FA),  $CH_3$ – (acetic acid, AA),  $CH_3CH_2$ – (propionic acid, PA) and  $CH_3CH_2CH_2$ – (butyric acid, BA)). Based on the obtained results, the length of the

\* Corresponding authors.

E-mail addresses: [zareiemedhi@gmail.com](mailto:zareiemedhi@gmail.com) (M. Zareie Yazdan-Abad), [mnoroofifar@chem.usb.ac.ir](mailto:mnoroofifar@chem.usb.ac.ir) (M. Noroozifar).

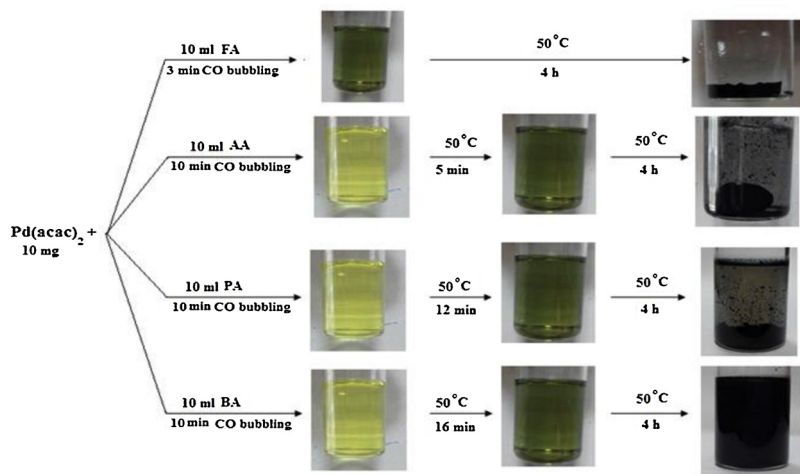


Fig. 1. Photographs of synthesis conditions of synthesized Pd aerogels in FA, AA, PA and BA solvents.

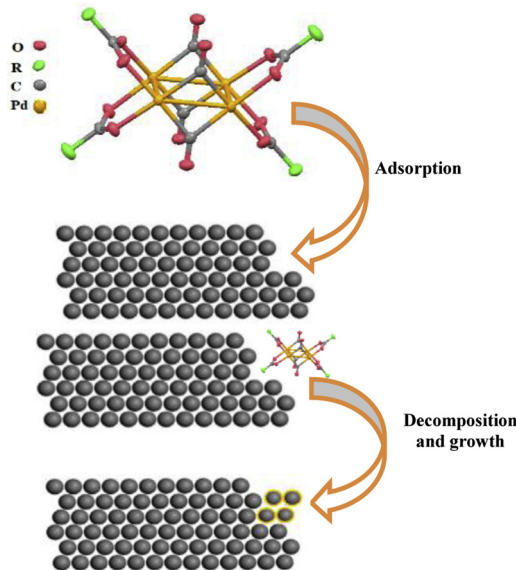


Fig. 2. Schematic illustration of the proposed formation of Pd nanosheets.

carbon chain in monocarboxylic acid plays an important role in the thickness of Pd nanosheets and the morphology of the as-prepared Pd aerogels. The electrocatalytic activities of Pd aerogels were evaluated using cyclic voltammetry (CV) and chronoamperometry (CA) experiments toward ethanol oxidation and the results were compared with the commercial Pd/C catalyst.

## 2. Experimental section

### 2.1. Synthesis of Pd aerogels

10 mg of palladium acetylacetonate ( $\text{Pd}(\text{acac})_2$ ) was dissolved in 10 mL of each carboxylic acid solvents in 15 mL glass vials. The mixture was bubbled with CO gas for a certain time. The bubbling time for FA is 3 min, and for other solvents, it is 10 min. After bubbling, the glass vial was immediately sealed and kept in 50 °C for 4 h without shaking. Then, the black hydrogel was immersed and washed in acetone for three times. The resulting anhydrous, acetone-containing Pd gels were transferred into a critical point dryer for supercritical  $\text{CO}_2$  drying. For the Atomic-force microscopy (AFM) analysis a suspension of Pd aerogel in ethanol was ultrasonic for 10 min to obtain a homogeneous black suspension. Then, 5  $\mu\text{l}$  of the suspension was placed on the silicon wafer

and was dried in the oven at 50 °C.

### 2.2. Instrumentation

To study the morphology of all aerogels, Transmission electron microscopy (TEM), Field Emission Scanning Electron Microscopy (FESEM) and Atomic force microscopy (AFM) were applied. FESEM and TEM were taken by using MIRA3 TESCAN and FEI Tecnai, respectively. The X-Ray Diffraction (XRD) patterns of all aerogels were achieved from an X-ray powder diffractometer (Philip X' Pert Pro MPP) at 20 angles from 30° to 85° by utilizing a Cu K $\alpha$  radiation ( $\lambda = 1.54056 \text{ \AA}$ ). AFMs were taken by using a DualScopeTM C-26 with a DME probe model DS 95-50-E.

### 2.3. Electrochemical measurements

Pd aerogel modified working electrodes were prepared by depositing aqueous dispersion of aerogels onto a glassy carbon (GC, with  $0.0314 \text{ cm}^{-2}$  surface areas) electrode followed by drying under ambient condition. A platinum wire and Hg/HgO (MMO) were utilized as the counter and reference electrodes, respectively. To evaluate the electrochemically active surface area of all aerogels, cyclic voltammetry (CV) experiments were carried out in 1.0 M NaOH solutions with a scan rate of 50 mV/s. For the electrooxidation process of ethanol, the cyclic voltammograms were conducted at a scan rate of 50 mV/s in 1.0 M NaOH + 1.0 M ethanol. All electro-chemical examinations were carried out at room temperature (RT).

## 3. Results & discussion

The Pd hydrogels synthesized in four carboxylic acid solvents including FA, AA, PA and BA in 4 h and 50 °C are shown in Fig. 1. In this study, Pd (FA), Pd (AA), Pd (PA) and Pd (BA) correspond to Pd aerogels synthesized in formic acid, acetic acid, propionic acid, and butyric acid, respectively. When  $\text{Pd}(\text{acac})_2$  is dissolved in the selected carboxylic acid, a bright yellow solution is obtained. After bubbling of carbon monoxide into the aforementioned solution, the bright yellow color of the solution was changed to dark green, implying that the reduction reaction has started. As shown in Fig. 1, the required times for color changing for FA, AA, PA, and BA solvents are 3, 5, 12 and 16 min, respectively. Actually, the reduction reaction time increases as the length of alkyl group increases (from FA to BA solvent).

From Fig. 1, it can be seen that the ability of the self-assembly process increases as the length of alkyl group decreases (from BA to FA solvent). Since the carbon chain in carboxylic acid solvents can act as capping agent, so, the self-assembly process is expected to be facilitated

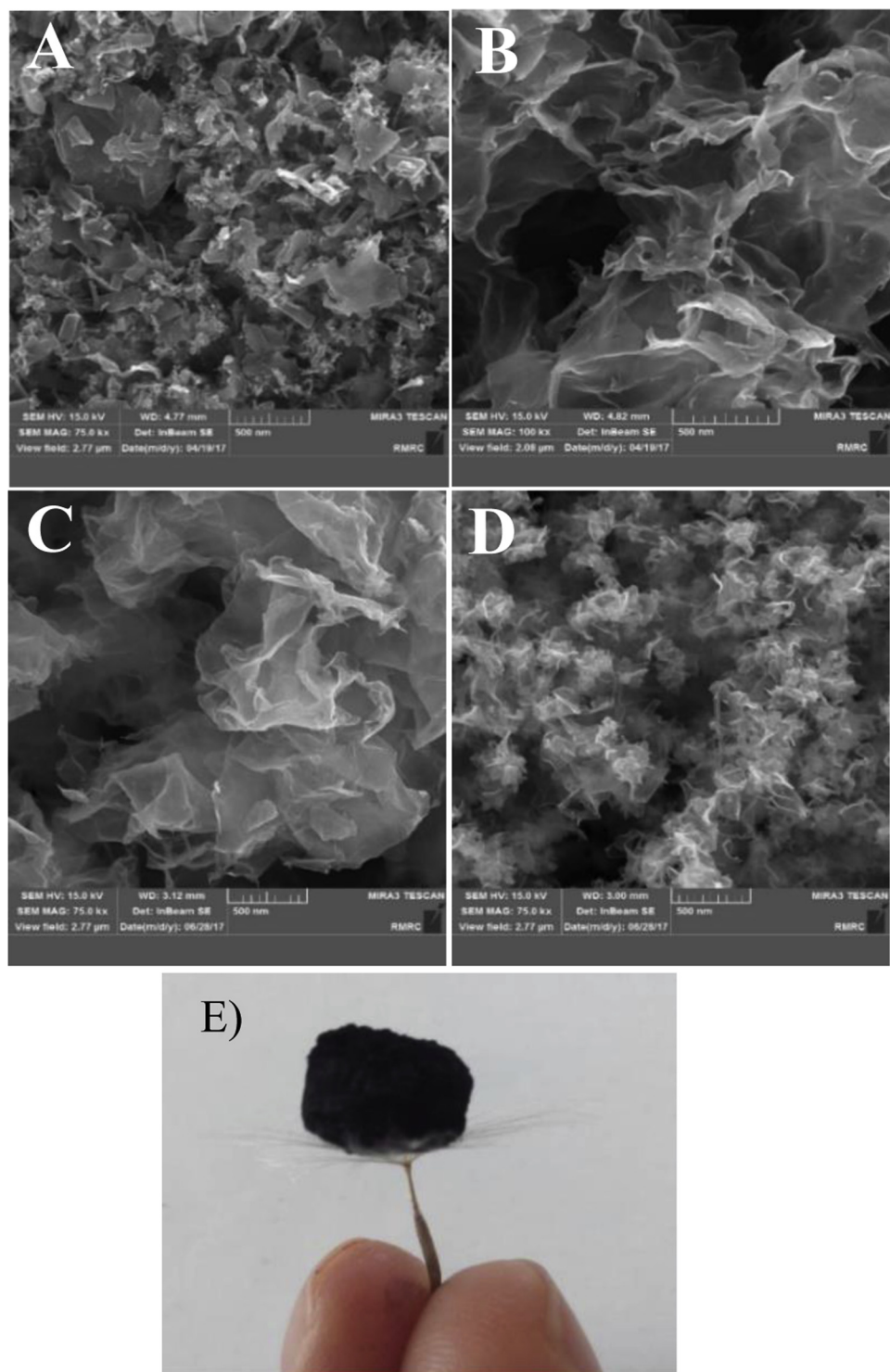


**Fig. 3.** FESEM images of A) Pd (FA), B) Pd (AA), C) Pd (PA), D) Pd (BA). E) A typical photograph of Pd aerogel synthesized in PA solvent balanced on the dandelion.

by decreasing the length of the carbon chain. When BA is used as the solvent, the Pd hydrogel is weakly formed since BA has an alkyl group with three carbon atoms that act as a mild capping agent and prevent the self-assembly process. While Pd hydrogel is strongly formed in the presence of FA solvent that has no alkyl group.

It has been proved that the  $\text{Pd}(\text{acac})_2$  dissolved in the AA solvent in the presence of CO gas, forms a complex  $(\text{Pd}_4(\text{CO})_4(\text{OAC})_4)$ , ( $\text{OAC} = \text{CH}_3\text{COO}^-$ ) [19]. This complex includes 4 Pd ions and 4 molecules of AA and carbon monoxide. It is proposed that a similar complex can be formed with other carboxylic acids. The proposed growth mechanism of

palladium nanosheets is illustrated in Fig. 2.

After the formation of the complexes, many of them are decomposed to atomic Pd clusters. Afterwards the residue complexes are adsorbed in the edge of atomic Pd clusters and are decomposed to four Pd atoms. This process will continue until the formation of nanosheets.

The R groups in the complex (Fig. 2) play a crucial role in the formation of Pd nanosheets and sheet thickness. When the R is  $\text{CH}_3^-$  and  $\text{CH}_3\text{CH}_2^-$  for AA and PA solvents, respectively, the uniform and extensive Pd nanosheets are formed, while for R = H (for FA) and  $\text{CH}_3\text{CH}_2\text{CH}_2^-$  (for BA), disordered structures are formed. The FESEM

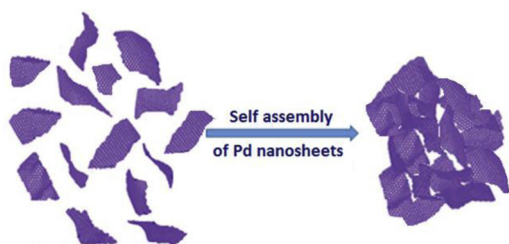


Fig. 4. Illustration of the self-assembly process of Pd nanosheets to the Pd aerogel.

was used to study the morphology of Pd aerogels, and the results are shown in Fig. 3. Among the carboxylic acid solvents, FA has no carbon chain; therefore, it cannot act as a capping agent, and when Pd clusters are generated in FA solvent, random collisions take place rapidly, and a nonuniform 3-D structure is formed.

When AA or PA is used as a solvent, a slow decomposition reaction occurs, and carbon chains act as a weak capping agent that allows the Pd clusters to go towards the formation of nanosheets. The best morphology is obtained when AA and PA are used as solvents. All FESEM images were taken with the same scale bare (500 nm) so that morphological differences could be clearly observed. As shown in Fig. 3B and C, the Pd aerogels assembled in AA and PA solvents show the uniform and extensive Pd nanosheets. Fig. 3E shows a typical photograph of Pd aerogel synthesized in AA solvent that is balanced on the dandelion.

It well confirms the ultralow density of the Pd aerogel synthesized by this method. Self-assembly process of Pd nanosheets towards the formation of Pd aerogels is depicted in Fig. 4. Self-assembly process was performed by interconnecting Pd nanosheets randomly, resulting in a high open pore 3-D macrostructure.

Fig. 5 (A, B) shows the TEM images of Pd aerogels synthesized in AA and PA solvents. TEM images revealed that due to their ultrathin feature, the Pd nanosheets become creased leading to the formation of a 3-

D structure.

The high-resolution TEM (HRTEM) images of Pd (AA) and Pd (PA) (Fig. 5C and D, respectively) show well-defined lattice fringes with an interplanar spacing of 0.23 nm which is in agreement with the lattice spacing of the (111) plane of face-center cubic-Pd (fcc-Pd) [20]. Based on the HRTEM image, it can be seen that the areas of Pd sheets are divided into crystalline and amorphous regions. The crystalline regions are welded by amorphous regions.

The thickness and surface roughness of the Pd nanosheets were studied by AFM. Fig. 6 (A, C) shows the AFM images of Pd aerogels synthesized in AA and PA solvents. These images depict a single Pd nanosheet on the silicon wafer. According to height profiles in Fig. 6 (B, D), the thickness of Pd nanosheets synthesized in AA and PA solvents are 6.89 and 1.94 nm, respectively. The capping ability of PA solvent is little more than that of AA solvent. Therefore, PA solvent prevents the growth of nanosheets in thickness leading to the formation of ultrathin Pd nanosheets (1.94 nm). As a result, it can be found that the length of the carbon chain in carboxylic acid solvents plays an important role in the thickness of Pd nanosheets.

The crystal structures of Pd aerogels synthesized in AA and PA solvents are determined by XRD (See Fig. 7).

There are four distinctive diffraction peaks at ca. 40°, 46°, 68° and 82° related to the face-centered cubic (fcc) phase of palladium. The intensities of the (111) phase for both aerogels are larger than those of other phases. It is found that the (111) phase of Pd catalyst is more suitable for fuel cell application because this phase is less prone to oxidation [21]. The hierarchical porous structures of the as-prepared Pd aerogels assembled by Pd nanosheets possess unique properties including 1) large surface area, 2) efficient mass transport through the pores and easier access to active sites, and 3) self-supporting character leading to prevent the loss of durability. Hence, it is interesting to study the catalytic activity of these Pd aerogels toward electrooxidation of ethanol.

The electrocatalytic behaviors of all aerogels were investigated by using cyclic voltammetry (CV) at room temperature (RT) with the same Pd loading in 1.0 M NaOH solution with a scan rate of 50 mVs<sup>-1</sup>

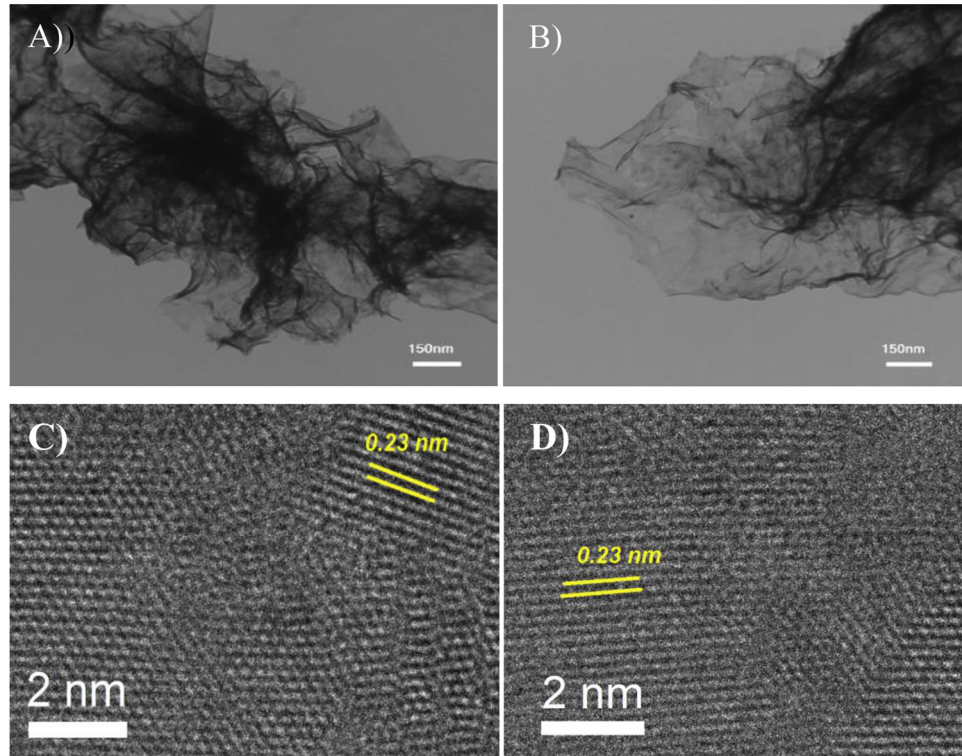


Fig. 5. TEM images of A) Pd (AA) and B) Pd (PA); HRTEM images of C) Pd (AA) and D) Pd (PA).

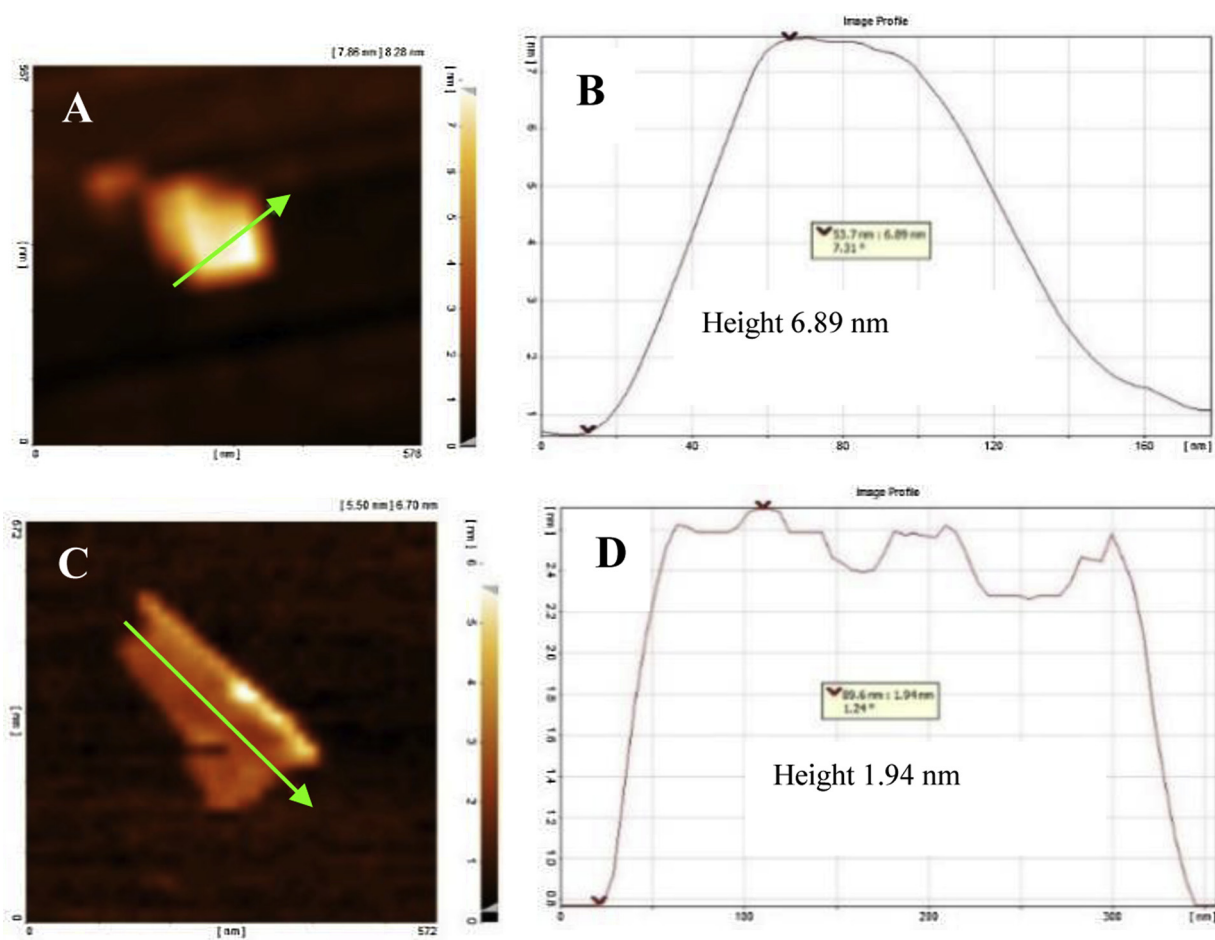


Fig. 6. A) AFM image and B) height of Pd aerogel synthesized in AA solvent; C) AFM image, and D) height of Pd aerogel synthesized in PA solvent.

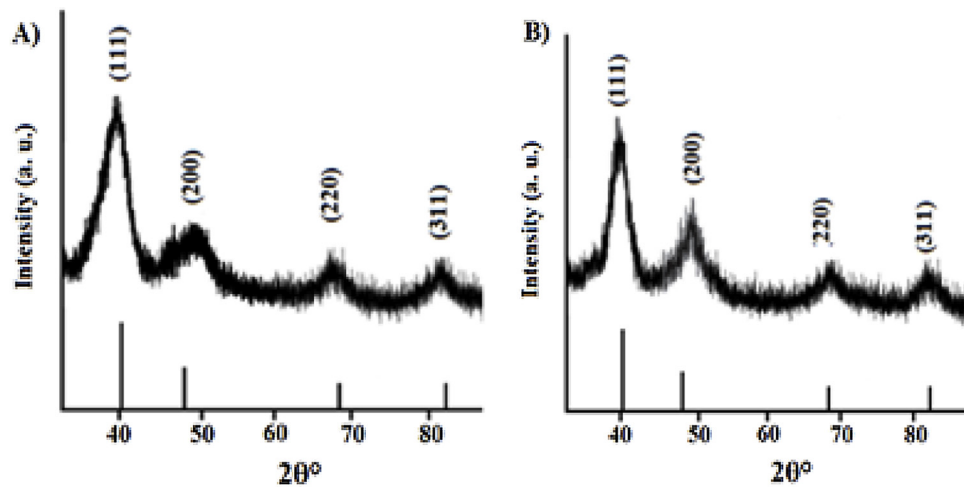


Fig. 7. XRD patterns of A) Pd (AA) and B) Pd (PA).

(Fig. 8).

The electrochemically active surface area (ECSA) of all aerogels can be measured from the area of the reduction peak of PdO which is an excellent index for the assessment of active sites of the catalysts in accordance with the following equation [22–26]:

$$\text{ECSA} = Q / (0.405 \times \text{Pd}_m)$$

where,  $Q$  is the columbic charge in mC and is calculated for all aerogels by integrating the charges associated with the peak reduction of PdO in

Fig. 8, a constant, assuming  $(0.405 \text{ mCcm}^{-2})$  the charge required for the reduction of a PdO monolayer and  $\text{Pd}_m$  refers to the Pd loading ( $\text{mgcm}^{-2}$ ) on the electrode surface. The values of ECSA for Pd aerogels synthesized in different carboxylic acid solvents were obtained 33.5, 82.5, 81.8 and 52.7  $\text{m}^2/\text{g}$  for FA, AA, PA and BA aerogels, respectively, which are much higher compared to the commercial Pd/C catalyst ( $14.3 \text{ m}^2/\text{g}$ ). The highest ECSA for Pd (AA) and Pd (PA) can be attributed to the uniform and extensive nanosheets in their textures. Fig. 9A compares the electrocatalytic activities of the as-synthesized Pd(FA), Pd

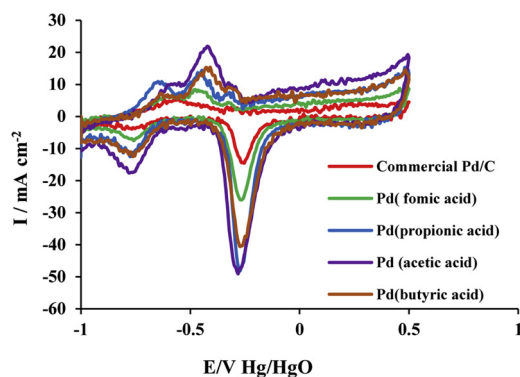


Fig. 8. CV curves of Pd aerogels and commercial Pd/C electrodes in 1.0 M NaOH at a scan rate of  $50 \text{ mVs}^{-1}$ .

(AA), Pd(PA), Pd(BA) and commercial Pd/C catalysts toward ethanol oxidation reaction (EOR) by using the CV technique at RT in the mixture of 1.0 M NaOH and 1.0 M  $\text{C}_2\text{H}_5\text{OH}$  aqueous solution at a scan rate of  $50 \text{ mVs}^{-1}$ . For each catalyst, there is an obvious oxidation peak in both forward and backward scans, respectively. The forward anodic peak current density ( $J_f$ ) reflects the amount of ethanol oxidized on the active sites of electrocatalysts.

The electro-oxidation process of ethanol goes along with the production and adsorption of intermediate species on the active sites. In the backward scans, because of the oxidation and removal of incompletely oxidized intermediates, a backward peak current density ( $J_b$ ) is observed. Therefore, the ratio of forward peak current density ( $J_f$ ) to backward peak current density ( $J_b$ ) is primarily utilized to study the tolerance of the catalyst to agglomeration of intermediate species [27–29]. Therefore, a higher ratio of  $J_f/J_b$  is attributed to more efficient EOR and less aggregation of intermediate carbonaceous species on the surface of each catalyst. The  $J_f/J_b$  ratios for Pd (FA), Pd(AA), Pd(PA), Pd(BA) aerogels and commercial Pd/C catalyst are 1.38, 1.69, 1.72,

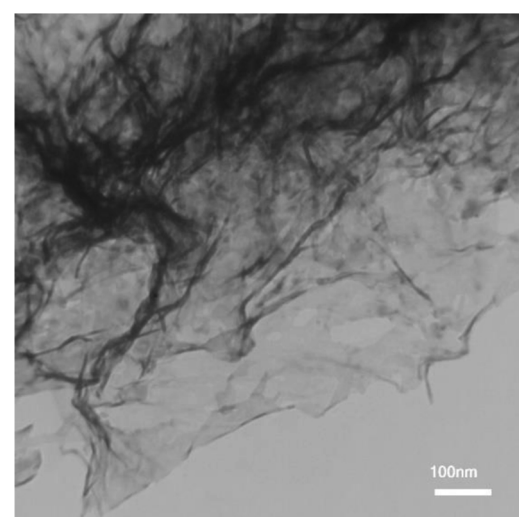


Fig. 10. TEM image of Pd(AA) after the CA test.

1.39 and 1.0, respectively.

As shown in Fig. 9A, the oxidation current densities on the Pd(FA), Pd(AA), Pd(PA) and Pd(BA) aerogels are 284, 533, 478 and  $380 \text{ mA cm}^{-2}$ , respectively, which are much higher than the commercial Pd/C ( $78.1 \text{ mA cm}^{-2}$ ). Moreover, all aerogels show a negative shift in the onset potential during the forward scan. All aerogels represent better electrocatalytic performances toward electrooxidation reaction of ethanol in comparison to the commercial Pd/C catalyst, which can be attributed to the high specific surface area and presence of large open pores leading to faster mass transport.

The CA measurements were utilized to evaluate the long-term stability of the Pd aerogels in 1.0 M NaOH + 1.0 M ethanol solution and were compared with the commercial Pd/C catalyst. As shown in Fig. 9B, at the early stage of the CA tests, all aerogels and commercial Pd/C

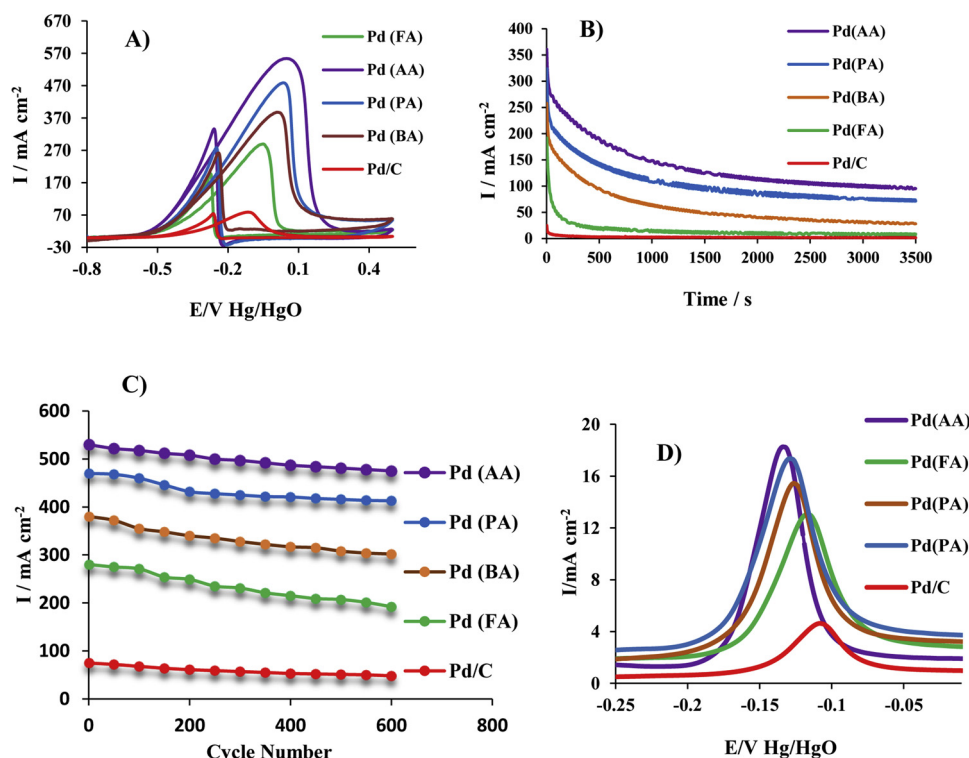


Fig. 9. A) CV curves and B) CA curves of Pd aerogels and commercial Pd/C electrodes in 1.0 M NaOH + 1.0 M  $\text{C}_2\text{H}_5\text{OH}$  solution; C) The cycling stability of peak current densities of the catalysts with increasing cycles; D) CO-stripping curves in 1 M NaOH solution at a scan rate of  $50 \text{ mVs}^{-1}$ .

**Table 1**

Comparison of specific activity of Pd and Pd-based nanoarchitectures toward ethanol oxidation in alkaline media.

Catalyst	Electrolyte concentration (M)	Ethanol concentration (M)	Scan rate (mV/s)	Current density (mA/cm <sup>-2</sup> )	Ref
np-Pd <sub>75</sub> Au <sub>25</sub> <sup>a</sup>	1.0	1.0	50.0	6.95	[31]
Pd NWs <sup>b</sup>	1.0	1.0	50.0	70.0	[32]
AuPd@Pd CSNF <sup>c</sup>	0.1	1.0	50.0	12.50	[33]
Pd <sub>3</sub> Pb-P10s <sup>d</sup>	0.5	1.0	50.0	2.02	[34]
Pd NWAs <sup>e</sup>	1.0	1.0	50.0	83.9	[35]
PdAu NWAs	1.0	1.0	50.0	83.7	[35]
THH Pd NCs <sup>f</sup>	0.1	0.1	10.0	1.84	[36]
Pd(FA)	1.0	1.0	50.0	284.0	This work
Pd(PA)	1.0	1.0	50.0	478.0	This work
Pd(BA)	1.0	1.0	50.0	380.0	This work
Pd(AA)	1.0	1.0	50.0	533.0	This work

<sup>a</sup> Nanoporous PdAu.<sup>b</sup> Palladium nanowires.<sup>c</sup> Gold-palladium@ palladium core-shell nanoflowers.<sup>d</sup> Flower-like Pd<sub>3</sub>Pb nanocrystals formed within 10 s by polyol method.<sup>e</sup> Palladium nanowire arrays.<sup>f</sup> Tetrahedral Pd nanocrystals.

sample presented a high current density, which is attributed to the double layer charging and available numerous active sites of all catalysts. All aerogels and commercial Pd/C depicted a quick current decay at the beginning of the CA test. This rapid decay can be due to the generation of some poisonous intermediates generated during the incomplete EOR and then adsorbed on the catalysts surface, covering the active site surfaces. After dramatic decay in currents, all catalysts slowly achieved steady current status. The Pd aerogels synthesized in AA solvent (Pd(AA)) and PA solvent (Pd(PA)) assembled by wide Pd nanosheets show the higher current density compared to other catalysts.

The cycling stability of catalysts towards EOR are examined for 600 cycles in the mixture of a solution of 1.0 M NaOH + 1.0 M EtOH at the scan rate of 50 mVs<sup>-1</sup> and the I<sub>f</sub> values after each 50 cycles are recorded and plotted against the cycle number, as shown in Fig. 9C. Based on cycling stability test, the conservation rate of I<sub>f</sub> values after 600 cycles for Pd(FA), Pd(AA), Pd(PA), Pd(BA) aerogels and Pd/C are 89.6% and 87.8%, 79.4%, 68.5%, 64% respectively, indicating that the Pd(AA) and Pd(PA) catalysts have superior cycling stability for ethanol electrooxidation.

For investigation of poisoning tolerance of as-prepared catalysts to CO intermediate species, CO-stripping experiments were performed, and the results were compared with Pd/C catalyst. CO-stripping curves in 1 M NaOH solution, was recorded at the potential windows of -0.25 to 0.0 V with the scan rate of 50 mVs<sup>-1</sup> (Fig. 9D). An ideal EOR catalyst should be capable of cleaning the CO species adsorbed on the active sites at lower oxidation potentials [30]. In Fig. 4, the anodic peaks between -0.2–-0.05 V are related to electrooxidation of adsorbed CO to CO<sub>2</sub> on the catalysts. As can be seen, potential peaks for Pd(FA), Pd(AA), Pd(PA), Pd(BA) aerogels and Pd/C are -0.133, -0.128, -0.125, -0.116 and -0.107 V, respectively. Among all the samples, Pd(AA) and Pd(PA) catalysts have the lowest potential peaks indicating that the morphology of catalyst affects CO removal and the anti-toxic ability of Pd(AA) is powerful.

For investigation the stability of the morphology of Pd (AA) catalyst, TEM image was taken after CA test (Fig. 10). With the comparison of Fig. 10 and Fig. 5A it is concluded that the 3D morphology of the Pd(AA) remains constant after stability test.

Table 1 presents the specific activity of Pd and Pd-based nanoarchitectures for electrooxidation reaction of ethanol in alkaline media. As shown, compared to other nanoarchitectures, all aerogels synthesized in this work offer more specific activity due to exceptional characteristics related to aerogels. In addition, the aerogel synthesized in the acetic acid shows higher current density compared to other aerogels. The much higher catalytic activity and durability of Pd(AA)

and Pd(PA) catalysts can be ascribed to this fact they are assembled by extensive and thin Pd nanosheets that render high active sites. In addition, 3-D and porous character of all aerogels are caused by easier accessibility of reactants to the active sites.

#### 4. Conclusion

In summary, we have described a morphology engineering in the new class of Pd aerogels assembled by Pd nanosheets. In this work, Pd aerogels were synthesized in carboxylic acid solvents with different alkyl groups. It was found that the length of the alkyl group plays a vital role in the morphology of the Pd aerogels and the thickness of Pd nanosheets. The Pd aerogels synthesized in AA and PA solvents show better morphology compared to other aerogels due to their alkyl groups acting as a mild capping agent. The Pd aerogels were applied towards EOR and displayed extraordinary catalytic performance and durability compared to the commercial Pd/C catalyst. This research work highlights the natural potential of Pd aerogels assembled by extensive nanosheets with the best morphology as highly efficient electrocatalysts.

#### Acknowledgment

We gratefully acknowledge the financial support from the University of Sistan and Baluchestan.

#### References

- [1] M.K. Debe, Electrocatalyst approaches and challenges for automotive fuel cells, *Nature* 486 (2012) 43–51.
- [2] M. Zareie Yazdan-Abad, M. Noroozifar, N. Alfi, Investigation on the electrocatalytic activity and stability of three-dimensional and two-dimensional palladium nanostructures for ethanol and formic acid oxidation, *J. Colloid Interf. Sci.* 532 (2018) 485–490.
- [3] L. Zhang, L. Wan, Y. Ma, Y. Chen, Y. Zhou, Y. Tang, T. Lu, Crystalline palladium–cobalt alloy nanoassemblies with enhanced activity and stability for the formic acid oxidation reaction, *Appl. Catal. B: Environ.* 138–139 (2013) 229–235.
- [4] Z. Qi, J. Weissmüller, Hierarchical nested-network nanostructure by dealloying, *ACS Nano* 7 (2013) 5948–5954.
- [5] B.Y. Xia, H.B. Wu, X. Wang, X.W. Lou, One-pot synthesis of cubic PtCu<sub>3</sub> nanocages with enhanced electrocatalytic activity for the methanol oxidation reaction, *J. Am. Chem. Soc.* 134 (2012) 13934–13937.
- [6] C. Zhongwei, W. Mahesh, L. Wenzhen, Y. Yushan, Supportless Pt and PtPd nanotubes as electrocatalysts for oxygen-reduction reactions, *Angew. Chem. Int. Ed.* 46 (2007) 4060–4063.
- [7] A. Shafaei Douk, M. Farsadrooh, F. Damanigol, A.R. Ansari Moghaddam, H. Saravani, M. Noroozifar, Porous three-dimensional network of Pd–Cu aerogel toward formic acid oxidation, *RSC Adv.* 8 (2018) 23539–23545.
- [8] D. Wen, A.K. Herrmann, L. Borchardt, F. Simon, W. Liu, S. Kaskel, A. Eychmüller, Controlling the growth of palladium aerogels with high-performance toward biocatalytic oxidation of glucose, *J. Am. Chem. Soc.* 136 (2014) 2727–2730.
- [9] C. Zhu, Q. Shi, S. Fu, J. Song, H. Xia, D. Du, Y. Lin, Efficient synthesis of MCu (M =

Pd, Pt, and Au) aerogels with accelerated gelation kinetics and their high electrocatalytic activity, *Adv. Mater.* 28 (2016) 8779–8783.

[10] D. Wen, W. Liu, D. Haubold, C. Zhu, M. Oschatz, M. Holzschuh, A. Wolf, F. Simon, S. Kaskel, A. Eychmüller, Gold aerogels: three-dimensional assembly of nanoparticles and their use as electrocatalytic interfaces, *ACS Nano* 10 (2016) 2559–2567.

[11] N.C. Bigall, A.-K. Herrmann, M. Vogel, M. Rose, P. Simon, W. Carrillo-Cabrera, D. Dorfs, S. Kaskel, N. Gaponik, A. Eychmüller, Hydrogels and aerogels from noble metal nanoparticles, *Angew. Chem. Int. Ed.* 48 (2009) 9731–9734.

[12] M. Zareie Yazdan-Abad, M. Noroozifar, A.R. Modarresi-Alam, H. Saravani, Palladium aerogel as a high-performance electrocatalyst for ethanol electro-oxidation in alkaline media, *J. Mater. Chem. A* 5 (2017) 10244–10249.

[13] W. Liu, A.-K. Herrmann, D. Geiger, L. Borchardt, F. Simon, S. Kaskel, N. Gaponik, A. Eychmüller, High-performance electrocatalysis on palladium aerogels, *Angew. Chem. Int. Ed.* 51 (2012) 5743–5747.

[14] A. Shafaei Douk, H. Saravani, M. Noroozifar, Three-dimensional assembly of building blocks for the fabrication of Pd aerogel as a high performance electrocatalyst toward ethanol oxidation, *Electrochim. Acta* 275 (2018) 182–191.

[15] H. Xu, P. Song, J. Wang, Y. Shiraishi, Y. Du, Q. Liu, Visible-light-driven 3D dendritic PtAu@Pt core-shell photocatalyst towards liquid fuel electrooxidation, *ACS Sustainable Chem. Eng.* 6 (2018) 7159–7167.

[16] B. Cai, A. Dianat, R. Hübner, W. Liu, D. Wen, A. Be-nad, L. Sonntag, T. Gemming, G. Cuniberti, A. Eychmüller, Shape engineering of the building blocks for efficient electrocatalysis, *Adv. Mater.* 29 (2017) 1605254.

[17] W. Yang, X. Zhang, Y. Xie, Advances and challenges in chemistry of two-dimensional nanosheets, *Nano Today* 11 (2016) 793–816.

[18] Y. Weiwei, G. Chengzhen, H. Di Feng, C.F. Qiang, Strong and conductive double-network graphene/PVA gel, *RSC Adv.* 4 (2014) 39588–39595.

[19] X. Yin, X. Liu, Y.T. Pan, K.A. Walsh, H. Yang, Ha-noi tower-like multilayered ultrathin palladium nanosheets, *Nano Lett.* 14 (2014) 7188–7194.

[20] S. Li, H. Yang, H. Zou, M. Yang, X. Liu, J. Jin, J. Ma, Palladium nanoparticles anchored on the NCNTs@NGS with a three-dimensional sandwich-stacked framework as an advanced electrocatalyst for ethanol oxidation, *J. Mater. Chem. A* 6 (2018) 14717–14724.

[21] M. Baldauf, D.M. Kolb, Formic acid oxidation on ultrathin Pd films on Au(hkl) and Pt(hkl) electrodes, *J. Phys. Chem.* 27 (1996) 11375–11381.

[22] N. Alfi, A.R. Rezvani, M. Khorasani-Motlagh, M. Noroozifar, Synthesis of europium oxide-promoted Pd catalyst by an improved impregnation method as a high performance catalyst for the ethanol oxidation reaction, *New J. Chem.* 41 (2017) 10652–10658.

[23] H. Yang, Z. Yu, S. Li, Q. Zhang, J. Jin, J. Ma, Ultrafine palladium-gold-phosphorus ternary alloyed nanoparticles anchored on ionic liquids-noncovalently functionalized carbon nanotubes with excellent electrocatalytic property for ethanol oxidation reaction in alkaline media, *J. Catal.* 353 (2017) 256–264.

[24] H. Yang, H. Zou, M. Chen, S. Li, J. Jin, J. Ma, The green synthesis of ultrafine palladium–phosphorus alloyed nanoparticles anchored on polydopamine functionalized graphene used as an excellent electrocatalyst for ethanol oxidation, *Inorg. Chem. Front.* 4 (2017) 1881–1887.

[25] N. Alfi, A.R. Rezvani, M. Khorasani-Motlagh, M. Noroozifar, A facile route for the preparation of new Pd/La<sub>2</sub>O<sub>3</sub> catalyst with the lowest palladium loading by a new reduction system as a high performance catalyst towards ethanol oxidation, *Int. J. Hydrogen Energy* 42 (2017) 18991–19000.

[26] M. Farsadrooh, J. Torrero, L. Pascual, M.A. Peña, M. Retuerto, S. Rojas, Two-dimensional Pd-nanosheets as efficient electrocatalysts for ethanol electrooxidation. Evidences of the C–C scission at low potentials, *Appl. Catal. B: Environ.* 237 (2018) 866–875.

[27] M. Zareie Yazdan-Abad, M. Noroozifar, N. Alfi, A.R. Modarresi-Alam, H. Saravani, Pd nanonetwork decorated on rGO as a high-performance electrocatalyst for ethanol oxidation, *Appl. Surf. Sci.* 462 (2018) 112–117.

[28] N. Alfi, M. Zareie Yazdan-Abad, A.R. Rezvani, M. Noroozifar, M. Khorasani-Motlagh, Three-dimensional Pd–Cd nanonetwork decorated on reduced graphene oxide by a galvanic method as a novel electrocatalyst for ethanol oxidation in alkaline media, *J. Power Sources* 396 (2018) 742–748.

[29] M. Zareie Yazdan-Abad, M. Noroozifar, N. Alfi, A.R. Modarresi-Alam, H. Saravani, A simple and fast method for the preparation of super active Pd/CNTs catalyst toward ethanol electrooxidation, *Int. J. Hydrogen Energy* 43 (2018) 12103–12109.

[30] H. Yang, X. Zhang, H. Zou, Z. Yu, S. Li, J. Sun, S. Chen, J. Jin, J. Ma, Palladium nanoparticles anchored on the three-dimensional nitrogen-doped carbon nanotubes as a robust electrocatalyst for ethanol oxidation, *ACS Sustainable Chem. Eng.* 6 (2018) 7918–7923.

[31] L.Y. Chen, N. Chen, Y. Hou, Z.C. Wang, S.H. Lv, T. Fujita, J.H. Jiang, A. Hirata, M.W. Chen, Geometrically controlled nanoporous PdAu bimetallic catalysts with tunable Pd/Au ratio for direct ethanol fuel cells, *ACS Catal.* 3 (2013) 1220–1230.

[32] Ch. Xu, H. Wang, P.K. Shen, S.P. Jiang, Highly ordered Pd nanowire arrays as effective electrocatalysts for ethanol oxidation in direct alcohol fuel cells, *Adv. Mater.* 19 (2007) 4256–4259.

[33] X. Qiu, Y. Dai, Y. Tang, T. Lu, Sh. Wei, Y. Chen, One-pot synthesis of gold–palladium@palladium core-shell nanoflowers as efficient electrocatalyst for ethanol electrooxidation, *J. Power Sources* 278 (2015) 430–435.

[34] R. Jana, U. Subbarao, S.C. Peter, Ultrafast synthesis of flower-like ordered Pd<sub>3</sub>Pb nanocrystals with superior electrocatalytic activities towards oxidation of formic acid and ethanol, *J. Power Sources* 301 (2016) 160–169.

[35] F. Cheng, X. Dai, H. Wang, S.P. Jiang, M. Zhang, Ch. Xu, Synergistic effect of Pd–Au bimetallic surfaces in Au-covered Pd nanowires studied for ethanol oxidation, *Electrochim. Acta* 55 (2010) 2295–2298.

[36] N. Tian, Z.-Y. Zhou, N.-F. Yu, L.-Y. Wang, Sh.-G. Sun, Direct electrodeposition of tetrahedahedral Pd nanocrystals with high-index facets and high catalytic activity for ethanol electrooxidation, *J. Am. Chem. Soc.* 132 (2010) 7580–7581.